Archival Report

Biological Psychiatry

Cumulative Effects of Social Stress on Reward-Guided Actions and Prefrontal Cortical Activity

Florent Barthas, Melody Y. Hu, Michael J. Siniscalchi, Farhan Ali, Yann S. Mineur, Marina R. Picciotto, and Alex C. Kwan

ABSTRACT

BACKGROUND: When exposed to chronic social stress, animals display behavioral changes that are relevant to depressive-like phenotypes. However, the cascading relationship between incremental stress exposure and neural dysfunctions over time remains incompletely understood.

METHODS: We characterized the longitudinal effect of social defeat on goal-directed actions and prefrontal cortical activity in mice using a novel head-fixed sucrose preference task and two-photon calcium imaging.

RESULTS: Behaviorally, stress-induced loss of reward sensitivity intensifies over days. Motivational anhedonia, the failure to translate positive reinforcements into future actions, requires multiple sessions of stress exposure to become fully established. For neural activity, individual layer 2/3 pyramidal neurons in the cingulate and medial secondary motor subregions of the medial prefrontal cortex have heterogeneous responses to stress. Changes in ensemble activity differ significantly between susceptible and resilient mice after the first defeat session and continue to diverge following successive stress episodes before reaching persistent abnormal levels.

CONCLUSIONS: Collectively, these results demonstrate that the cumulative impact of an ethologically relevant stress can be observed at the level of cellular activity of individual prefrontal neurons. The distinct neural responses associated with resilience versus susceptibility suggests the hypothesis that the negative impact of social stress is neutralized in resilient animals, in part through an adaptive reorganization of prefrontal cortical activity.

Keywords: Chronic stress, Goal-directed behavior, Prefrontal cortex, Pyramidal neurons, Reward, Social defeat

https://doi.org/10.1016/j.biopsych.2020.02.008

Stress is associated with increased risk for multiple neuropsychiatric disorders, including major depression (1). A prevailing framework for stress-related disorders is the idea of allostatic load, which posits that although acute stress may promote adaptation, repeated exposures over a prolonged period of time can lead to persistently heightened reactions and maladaptations (2,3). Accordingly, there is growing evidence that acute and chronic stress are associated with distinct alterations in the mammalian brain (4,5). However, effects of stress on behavior and neural functions are generally sampled at the beginning and end of chronic stress exposure, whereas the adaptations across successive stress episodes are not understood. One difficulty is that individuals may exhibit different degrees of resilience, and therefore, their time-dependent responses to repeated stress may be variable. Another difficulty is that longitudinal measurements are needed to track the dynamic relationship. For example, depressive-like phenotypes in rodents are thought to arise only after chronic stress, yet the timing of when the dysfunction is precipitated remains poorly understood.

In this study, we characterize the time course of stress effects on motivated behavior and prefrontal cortical activity in mice. Motivated behavior—specifically the capacity to select appropriate actions based on reinforcing outcomes—is an essential aspect of learning. Deficits in reward-guided behavior can be quantified precisely using instrumental decision-making tasks in multiple animal species and therefore have translational significance (6). For example, in humans, stress blunts goal-directed actions and promotes habitual responses (7). In agreement, rodents subjected to chronic stress paradigms exhibit a diminished ability to modify actions flexibly in an outcome-dependent manner (8–11).

A classic assay to measure reward-guided behavior in stressed rodents is the two-bottle test of sucrose preference, which is reduced following chronic stress (12,13). However, reduced preference can arise for at least two reasons. First, animals could be impaired in their ability to sense or gain pleasure from sucrose. This would relate to the emotional reactivity to the reward. Second, the sucrose may remain desirable, but animals could fail to translate that positive reinforcement into future actions. These two components of reward-guided behavior are well known, and the corresponding deficits have been termed "appetitive anhedonia" and

SEE COMMENTARY ON PAGE 514

ISSN: 0006-3223

"motivational anhedonia" (14,15). Unfortunately, the conventional sucrose preference metric does not dissociate these two forms of reward-processing deficits (16), so a more sophisticated paradigm is necessary to dissect the stress-induced behavioral alterations.

Reward-guided behavior is thought to involve the distributed cortical-basal ganglia network including the prefrontal cortex (6). In addition to deficits in reward processing, the effects of chronic stress on the prefrontal cortex can be detected at many levels, including morphological, molecular, and cellular (4,5). For example, in rodents, prolonged stress exposure causes structural atrophy, including dendritic retraction and synapse loss (8,17,18), and disrupts synaptic plasticity and synaptic transmission in the medial prefrontal cortex (mPFC) (19,20). Although it is obvious that the structural and synaptic alterations must compromise prefrontal cortical function, how stress exposure modifies neural activity in vivo is less clear. There have been several studies of stress effects on cortical activity patterns (21–24), but they provide few details on the effect of escalating stress burden over time.

Given the gaps in our current knowledge, the main goal of this study is to determine how social stress influences reward-guided behavior and prefrontal cortical activity over time. Using a novel head-fixed sucrose preference test and longitudinal two-photon calcium imaging, we show a progressive emergence of motivational anhedonia and heterogeneous neural activity maladaptations as a function of cumulative social stress and resilience.

METHODS AND MATERIALS

Animals

We used male adult (2- to 6-month-old) mice. Behavioral experiments were performed using wild-type C57BL/6J mice (catalog no. 000664; Jackson Laboratory, Bar Harbor, ME). Imaging experiments were performed using heterozygous CaMKIIa-Cre mice (catalog no. 005359; Jackson Laboratory) or C57BL/6J mice. For social defeat, aggressive residents were male retired breeder CD-1 mice, Crl:CD1(ICR) (catalog no. 022; Charles River Laboratories, Wilmington, MA).

Surgery

The Supplement and previous publications (25,26) provide details of the surgery for head plate implant and imaging window installation. Briefly, we targeted the cingulate (Cg1) and medial secondary motor (M2) regions of the mPFC (anteroposterior = +1.5 mm and mediolateral = +0.4 mm relative to the bregma). To express genetically encoded calcium indicator in pyramidal neurons, we injected pAAV(AAV1)-hSyn1-Flex-mRuby2-GSG-P2A-GCaMP6s-WPRE-pA (Addgene, Watertown, MA) in CaMKII-Cre mice. In a subset of experiments, we injected pAAV(AAV1)-CaMKII-GCaMP6f-WPRE-SV40 (Penn Vector Core, Philadelphia, PA; or Addgene) in C57BL/6J mice.

Self-Paced, Instrumental Sucrose Preference Task

The head-fixed mouse was placed on a treadmill and positioned in front of a lick spout made by soldering together 3 blunted 20-gauge hypodermic needles. The spout could deliver independently 4 μL of 1 of 3 solutions: 0% sucrose (i.e., tap water), 3% sucrose (weight per volume), and 10% sucrose. During the task, the fluid-restricted mouse must make 10 licks onto the spouts (FR10) to receive 4 μL of fluid reinforcement. Following the fluid delivery, there was a 5-second timeout period (FI5) during which licks do not count toward next FR10. The reinforcement type cycled from 0%, 3%, 10%, to 3% in a block design with 1-minute blocks. For details of the task design and analyses of behavioral data, see the Supplement.

Repeated Social Defeat

We followed published procedures to induce social defeat stress (27). Note that this protocol was milder than social defeat protocols in other studies (12,28), because the time for sensory interaction was shorter. For details, see the Supplement.

Two-Photon Imaging

The laser-scanning two-photon microscope was equipped with a resonant scanner unit for imaging at a frame rate of 29.8 Hz (Movable Objective Microscope; Sutter Instrument, Novato, CA). The Supplement provides details of the imaging setup and analyses.

Data Availability

The behavioral and imaging data, as well as MATLAB (The MathWorks, Inc., Natick, MA) code, are available on GitHub (https://github.com/Kwan-Lab/barthas2020).

RESULTS

A Self-Paced, Instrumental Sucrose Preference Task for the Head-Fixed Mouse

We designed a self-paced, instrumental sucrose preference task to characterize reward-directed actions. We had three major criteria for the task: 1) actions are self-paced to engage voluntary behavior; 2) sucrose reinforcements are varied to manipulate the motivational level; and 3) animal is head-fixed to enable cellular-resolution optical imaging, but mobile to minimize stress during behavioral testing. To meet these criteria, we incorporated concepts from prior studies involving ratio schedules (29), incentive contrast (30,31), and treadmill (32). During the task, the fluid-restricted mouse makes tongue licks on a spout and is reinforced on a tandem FR10-FI5 schedule (Figure 1A, B). The FI5 schedule is effectively a 5-second timeout after the reinforcement to avoid counting consummatory licks toward the subsequent FR10 schedule. The spout can independently deliver 4 μL of water, 3% sucrose, or 10% sucrose solution. For simplicity, we will refer to water as 0% sucrose solution. The task employs a block design (Figure 1C). Each block lasts 60 seconds and is associated with 1 fluid type, always going from 0% to 3% to 10% to 3%, and then the sequence repeats again. Cycling through the fluid types allows the study of relative reward values, because a 3% block preceded by a 0% block has different successive incentive contrast compared with a 3% block preceded by a 10% block. We refer to these 2 kinds of 3% blocks as 3% positive contrast (3% pc) and 3% negative contrast (3% nc) blocks. Overall, the self-paced, instrumental sucrose

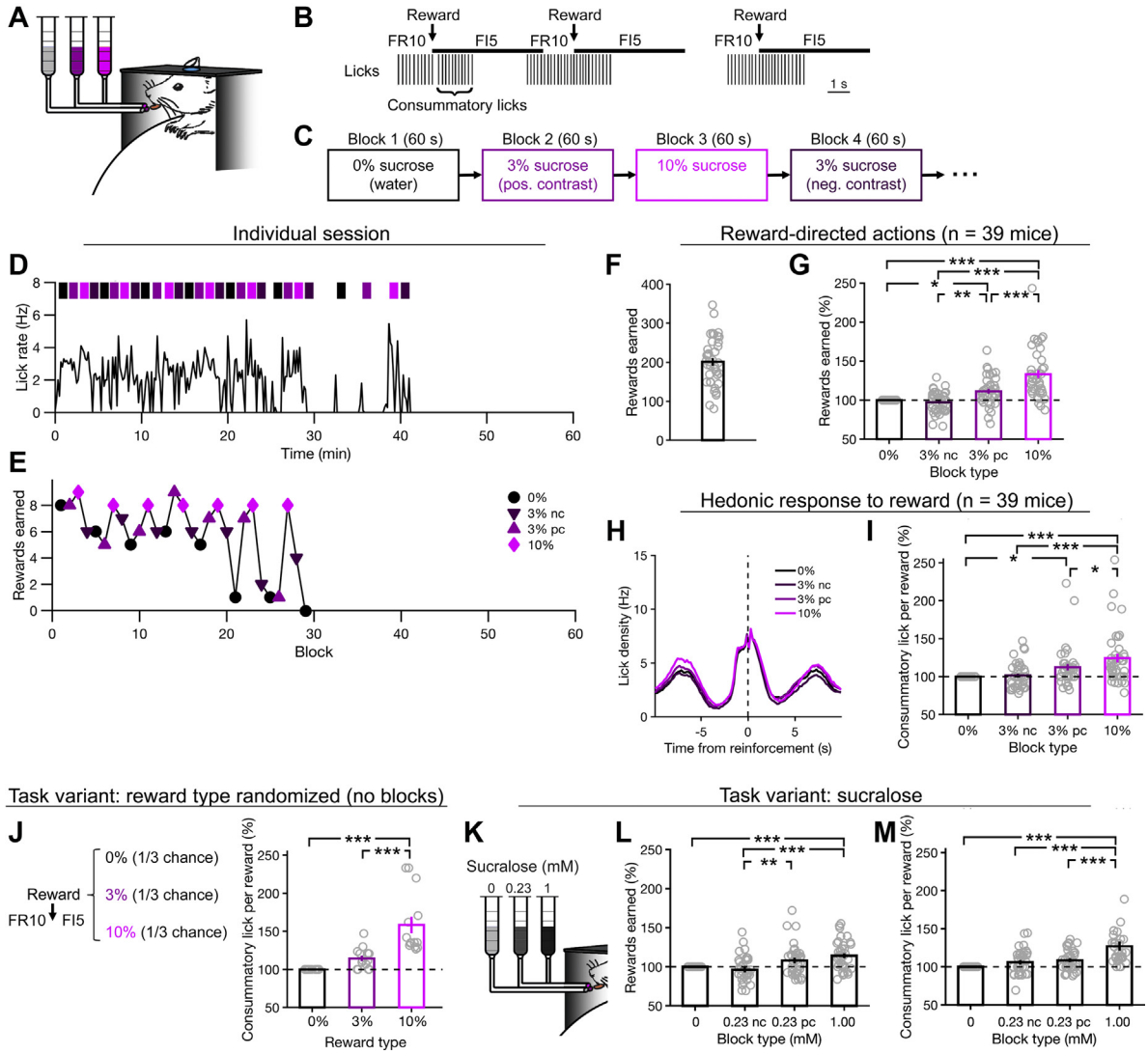

Figure 1. A self-paced, instrumental sucrose preference task for the head-fixed mouse. **(A)** Schematic of the experimental setup. The head-fixed mouse had access to a composite lick spout with 3 openings, each of which could deliver fluid independently. The mouse sat atop a skewered sphere or a treadmill and could run forward or backward. **(B)** The task was based on a tandem fixed-ratio (FR), fixed-interval (FI) schedule. To illustrate the FR10-FI5 schedule, licks detected and reinforcement delivered from an actual behavioral session are plotted. **(C)** The task had a block design, cycling through multiple types of reinforcement including 0%, 3%, and 10% sucrose solutions. The sequence was always 0%, 3%, 10%, 3%, and then 0%, 3%, 10%, 3% again, and so on. **(D)** Lick rate for a typical session. Lick rate was calculated in 10-second bins. The colored patches indicated the reinforcement type and duration of the blocks. Note that there were time gaps between the blocks, because a new block would begin only after the completion of a FR10 action sequence. The mouse responded for about 30 minutes before stopping due to satiation. **(E)** Rewards earned for each block. This is the same session as in **(D)**. **(F)** Rewards earned per session. Open circles, individual sessions; bar, mean ± SEM. **(G)** Rewards earned for each reinforcement type, normalized by rewards earned in 0% blocks, per session. Open circles, individual sessions; bar, mean ± SEM. Main effect of reinforcement type ($F_{3,114} = 47.8$; $p = 4 \times 10^{-20}$), comparisons: 0% vs. 3% positive contrast (pc), $p = .012$; 0% vs. 10%, $p = 4 \times 10^{-9}$; 3% negative contrast (nc) vs. 3% pc, $p = .0011$; 3% nc vs. 10%, $p = 4 \times 10^{-9}$; 3% pc vs. 10%, $p = 1 \times 10^{-7}$, analysis of variance (ANOVA) with post hoc Tukey-Kramer test. **(H)** Mean lick density relative to the time of reinforcement, plotted separately for each reinforcement type. **(I)** Consummatory licks per reward for each reinforcement type, normalized by the number in 0% blocks. Open circles, individual sessions; bar, mean ± SEM. Main effect of reinforcement type ($F_{3,114} = 9.0$; $p = 6 \times 10^{-8}$), comparisons: 0% vs. 3% pc, $p = .02$; 0% vs. 10%, $p = 5 \times 10^{-7}$; 3% nc vs. 10%, $p = 2 \times 10^{-6}$; 3% pc vs. 10%, $p = .03$, ANOVA with post hoc Tukey-Kramer test. **(J)** A separate cohort of mice was trained on a variant of the task with the same FR10-FI5 schedule; however, reinforcement type was randomized for each reward. Open circles, individual sessions; bar, mean ± SEM. Main effect of reinforcement type ($F_{2,26} = 25.0$; $p = 9 \times 10^{-7}$), comparisons: 0% vs. 10%, $p = 8 \times 10^{-7}$; 3% vs. 10%, $p = 1 \times 10^{-4}$, ANOVA with post hoc Tukey-Kramer test. **(K)** Another separate cohort of mice was trained on a variant of task in which the reinforcement types were 0, 0.23, and 1 mM sucralose. **(L)** Similar to **(H)** except for sucralose task. Main effect of reward type ($F_{3,105} = 10.6$; $p = 4 \times 10^{-6}$), comparisons: 0 vs. 1.00, $p = .0006$; 0.23 nc vs. 0.23 pc, $p = .006$; 0.23 nc vs. 1.00, $p = 8 \times 10^{-6}$, ANOVA with post hoc Tukey-Kramer test. **(M)** Similar to **(I)** except for sucralose task. Main effect of reward type ($F_{3,105} = 15.9$; $p = 1 \times 10^{-8}$), comparisons: 0 vs. 1.00, $p = 2 \times 10^{-8}$; 0.23 nc vs. 1.00, $p = 9 \times 10^{-6}$; 0.23 pc vs. 1.00, $p = 1 \times 10^{-4}$, ANOVA with post hoc Tukey-Kramer test. Sample sizes were 39 sessions from 39 mice **(F–I)**, 14 sessions from 2 mice **(J)**, and 39 sessions from 9 mice **(K–M)**. $^{*}p < .05$, $^{**}p < .01$, $^{***}p < .001$. In the list above, if a potential post hoc comparison was unnoted, $p \geq .05$.

preference task allows us to measure how an animal adjusts its actions in response to differences in absolute and relative reward values.

Mice Are Sensitive to Sucrose Concentration and Incentive Contrast

Figure 1D shows a typical behavioral session for an adult male C57BL/6J mouse. Plotting the number of rewards earned on a block-by-block basis revealed a sawtooth-shaped modulation, which matched the rises and falls of the sucrose concentration (Figure 1E). The mouse could suppress intake when they anticipate more palatable fluids in the near future (33) and therefore responded most vigorously for the 10% blocks. Summarizing performance from 39 mice, the mice earned 201 $\pm$ 10 reinforcements per session (mean $\pm$ SEM) (Figure 1F). Mice were motivated to complete more FR10 schedules to obtain more reinforcements during blocks with more palatable fluids ($p = 4 \times 10^{-20}$, main effect of block type, 1-way analysis of variance [ANOVA]) (Figure 1G), such that they obtained 33 $\pm$ 5% more rewards during 10% blocks relative to 0% blocks ($p = 4 \times 10^{-9}$, post hoc Tukey-Kramer test). Animals also responded significantly more during 3% pc blocks than 3% nc blocks ($p = .0011$, post hoc Tukey-Kramer test). Therefore, both absolute and relative differences in reward values were relevant for performance in this task. Because ratio schedule is a well-known approach to induce goal-directed actions (29), these results emphasize the motivational component of responding.

Mice licked in bouts with a pause between successive reinforcements (Figure 1H). A typical bout would therefore include 10 licks to complete the fixed-ratio schedule, and then additional consummatory licks after reinforcement (11.0 $\pm$ 0.5 licks for water). Animals had more consummatory licks as the concentration of sucrose was increased ($p = 6 \times 10^{-8}$, main effect of block type, 1-way ANOVA) (Figure 1I). There is an extensive literature indicating that the number of consummatory licks is directly related to the emotional reaction to reinforcement (34,35). Results from task variants (Figure 1J–M; see the Supplement for details) confirmed that differences in consummatory licking arises from the appetitive component of responding and excluded caloric content as the factor underlying performance.

Motivational Anhedonia in Mice Susceptible to Social Defeat Stress

Although it is known that stress can induce anhedonia in rodents, the extent to which behavioral alterations can be attributed to the motivational versus appetitive components, as well as the time course of deficits, is not known. Social defeat stress has ethological relevance for animals (12) and is associated with maladaptations in the rodent frontal cortex (13,23,36). In these experiments (Figure 2A), C57BL/6J mice received 10 days of social defeat and were tested on the self-paced, instrumental sucrose preference task at 2-day intervals before, during, and after the defeat episodes.

The cohort tested included 28 stressed and 14 control mice. Results from social interaction tests confirmed that the defeat procedures led to a stress-dependent behavioral outcome (Figure 2B, C). We analyzed data from the self-paced, instrumental sucrose preference task during prestress (days -1 and 1), during-stress (days 5, 7, and 9), and poststress (days 11 and 13) stages. As expected, for control mice, rewards earned increased with sucrose concentration, and this motivational effect was stable across days ($p = 1 \times 10^{-8}$, main effect of reward type; ANOVA with block type and stage as fixed factors and subject as random factor) (Figure 2D). By contrast, susceptible mice had diminished sensitivity to both absolute and relative reward differences that persisted into the poststress stage ($p = 7 \times 10^{-8}$, main effect of reward type; $p = .003$, main effect of stage) (Figure 2E). Resilient mice also had reduced reward sensitivity, but the decrease was transient, as sucrose preference quickly returned to prestress level following the last defeat session (Figure 2F). Therefore, mice subjected to repeated social defeat displayed motivational anhedonia, with the susceptible subtypes displaying a more prolonged phenotype.

Delayed Emergence of Motivational Anhedonia From Cumulative Effects of Stress

To gain insight into the factors that drove the motivational anhedonia, we applied a computational model of response vigor (37,38). The total cost for performing a lick bout is a sum of the energetic cost of physical effort in performing actions in quick succession (37) and the opportunity cost of forgoing a reward by not performing an action (Figure 3A). Opportunity costs grow linearly as a function of latency between actions, with a rate for water rewards (k_o) and scaling factors to account for accelerated rates for other reinforcement types (c_{3nc}, c_{3pc}, c_{10}). Satiety is captured by marginal utility with exponentially diminishing returns (α), which occurs after a certain number of rewards (R_o). At any moment during the task, the goal of the mouse is to select a latency for the next lick bout to minimize the total cost.

The model was useful for distilling the session-by-session variations in behavioral performance into a few parameters. For each session, we fit the model to the behavioral data (Figure 3B, C). Focusing on susceptible mice, reward sensitivity was significantly modulated by reward type and day ($p = 3 \times 10^{-4}$, main effect of reward type; $p = 3 \times 10^{-6}$, main effect of day; ANOVA with block type and day as fixed factors and subject as random factor) (Figure 3D–F). Notably, the motivational deficit did not emerge immediately following the first few stress sessions, but rather became detectable starting on day 7. This stress-related blunting of motivational action was severe in susceptible mice, relative to the more variable effects in resilient mice (Figure 3G). By contrast, the threshold for marginal utility also increased after stress but did not depend on susceptibility (Figure 3H–J; see the Supplement for details). Appetitive anhedonia, as measured by consummatory licks, was induced by stress but only transiently (Figure 4; see the Supplement for details). Overall, for motivational anhedonia, the delayed emergence and protracted time course indicate that it is a consequence of the cumulative impact of the chronic stressor.

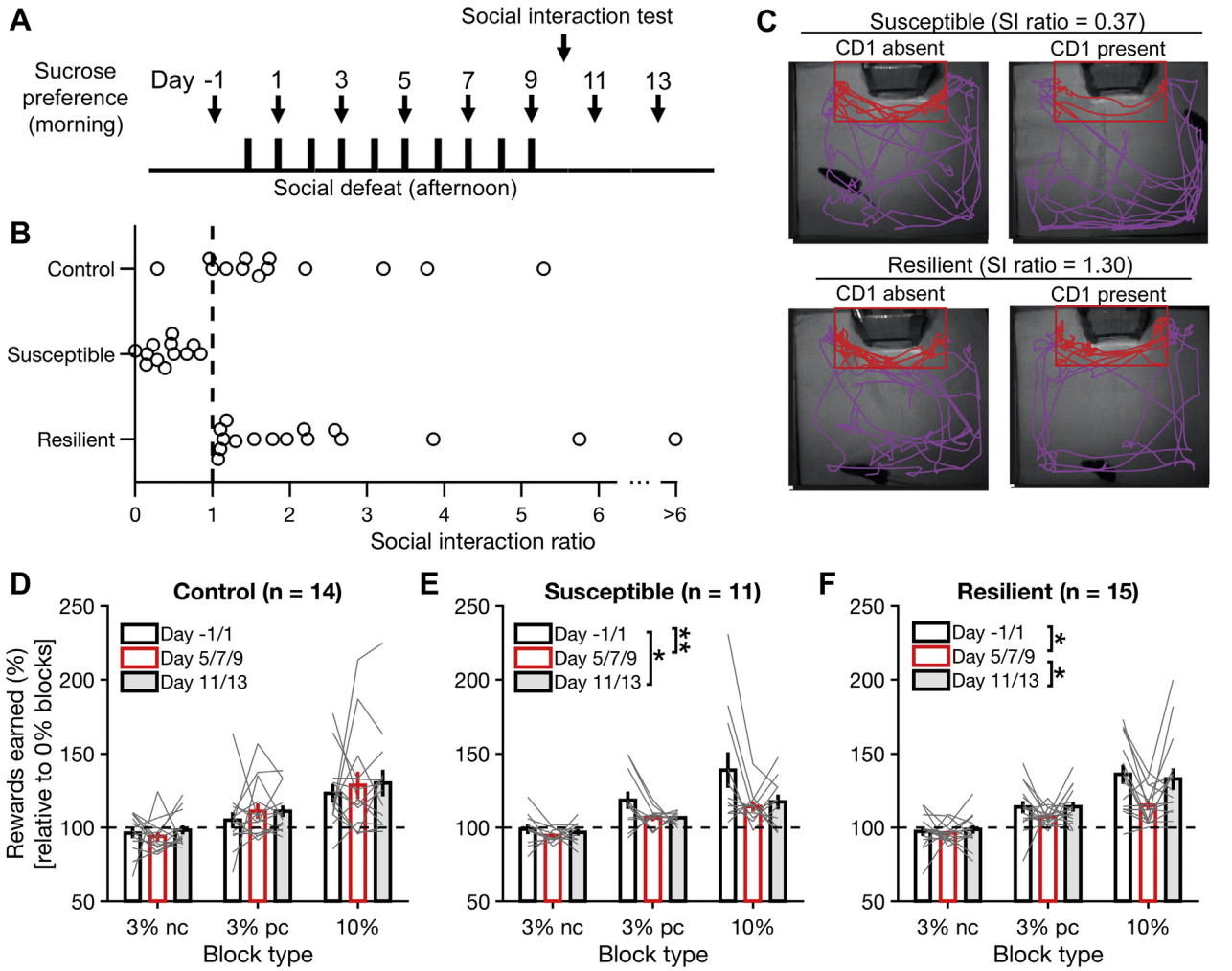

Figure 2. Motivational anhedonia as a sustained phenotype in susceptible, but not resilient, mice. **(A)** Timeline of the chronic social defeat stress and behavioral experiments. **(B)** Based on the social interaction (SI) ratio, mice subjected to social defeat were divided into resilient and susceptible mice. Control mice were handled but did not experience social defeat. Each circle in the bee swarm plot represents a mouse. **(C)** Example movement trajectories for a susceptible and a resilient mouse, when the CD1 aggressor mouse was present or absent in the interaction zone (red rectangle). **(D)** Rewards earned for each reinforcement type, normalized by rewards earned in 0% blocks, per session, for control mice. For each animal, the value was an average across days according to 3 stages: "pre" for days −1 and 1; "stress" for days 5, 7, and 9; and "post" for days 11 and 13. Gray line, individual animal; bar, mean ± SEM. Main effect of reinforcement type ($F_{2,117} = 21.4$, $p = 1 \times 10^{-8}$), but not for stage ($F_{2,117} = 0.57$, $p = .6$) or interaction ($F_{4,117} = 0.16$, $p = 1$), analysis of variance with reinforcement type and stage as fixed factors, subject as random factor. **(E)** Similar to **(D)** for susceptible animals. Main effect of reinforcement type ($F_{2,90} = 20.0$, $p = 7 \times 10^{-8}$) and stage ($F_{2,90} = 6.16$, $p = .003$), but not interaction ($F_{4,90} = 1.28$, $p = .3$), with comparisons: pre vs. stress, $p = .005$; pre vs. post, $p = .02$; stress vs. post, $p = .9$, analysis of variance with reinforcement type and stage as fixed factors, subject as random factor, and post hoc Tukey-Kramer test. **(F)** Similar to **(D)** for resilient mice. Main effect of reinforcement type ($F_{2,126} = 40.6$, $p = 3 \times 10^{-14}$), stage ($F_{2,126} = 5.05$, $p = .008$), but not interaction ($F_{4,126} = 1.70$, $p = .2$), with comparisons: pre vs. stress, $p = .013$; pre vs. post, $p = 1$; stress vs. post, $p = .02$, analysis of variance with reinforcement type and stage as fixed factors, subject as random factor, and post hoc Tukey-Kramer test. Sample sizes were 14 mice **(D)**, 11 mice **(E)**, and 15 mice **(F)**. $^{*}p < .05$, $^{**}p < .01$. nc, negative contrast; pc, positive contrast.

Prefrontal Cg1/M2 Region: Imaging the Time Course of Neural Activity Changes at Cellular Resolution

The behavioral analysis and particularly the modeling suggest a progressive emergence of motivational anhedonia. Where should one look for the accompanying neural alterations? In rodents, the Cg1 and M2 subregion, which constitutes the most dorsal aspect of mPFC (39), is important for the production of self-initiated (40,41) and reward-guided actions (26,42–44). Furthermore, Cg1/M2 is a target of stress, as identified by brainwide mapping of neuronal activation in a rodent model for depression (45), and its response to the fast-acting antidepressant ketamine (46–48).

Neuronal firing leads to somatic calcium transients in pyramidal neurons (49), which could be visualized using a fluorescent calcium indicator. We used a recently developed

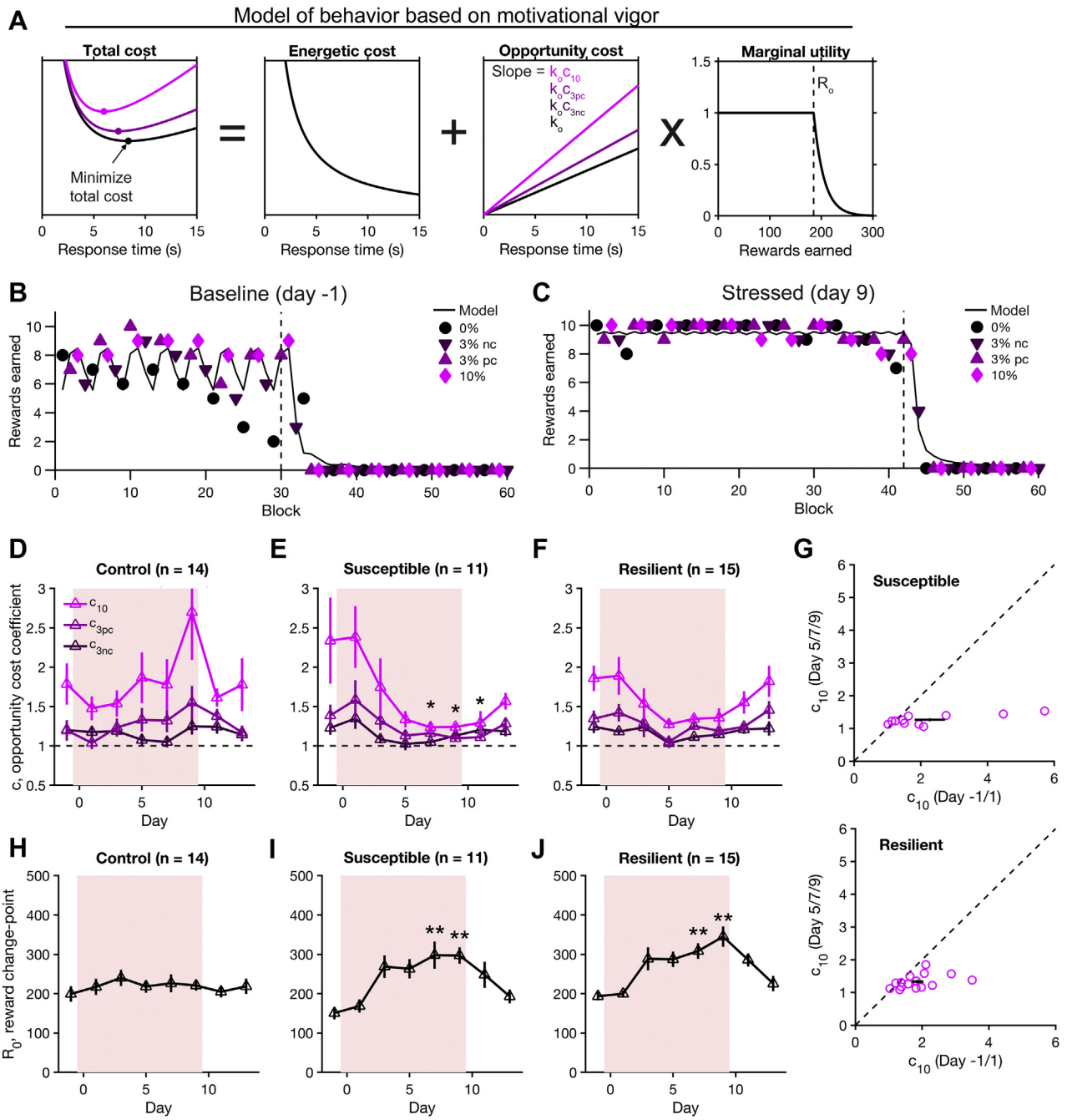

Figure 3. A model of self-paced, instrumental sucrose preference based on motivational vigor. **(A)** Schematic of the model. Animal should select a response time that minimizes the total cost. Total cost is the sum of an energetic cost, incurred if actions have to be performed in quick succession, and an opportunity cost, incurred when potential rewards are delayed due to inaction. The opportunity cost depends on the expected reinforcement type and a marginal utility term for diminishing returns due to satiation. From the optimal response time, we could estimate the number of completed actions per block. **(B)** Task performance and model fit for an example session on day −1. **(C)** Similar to **(B)** on day 9 for the same animal. **(D)** The opportunity cost coefficients determined by fitting model to individual sessions for control mice. Line, mean ±SEM. Shading, days with social defeat. Main effect of reinforcement type ($F_{2,305} = 14.0$, $p = 2 \times 10^{-6}$), but not for day ($F_{11,305} = 1.33$, $p = .2$) or interaction ($F_{22,305} = 0.541$, $p = 1$), analysis of variance (ANOVA) with reinforcement type and day as fixed factors, subject as random factor. **(E)** Similar to **(D)** for susceptible animals. Main effect of reinforcement type ($F_{2,269} = 8.43$, $p = 3 \times 10^{-4}$) and day ($F_{10,269} = 4.82$, $p = 3 \times 10^{-6}$), but not for interaction ($F_{20,269} = 0.983$, $p = .48$), ANOVA with reinforcement type and day as fixed factors, subject as random factor. Comparisons for the c_{10} parameter vs. day −1: $p = 1.0$ for day 1; $p = 1.0$ for day 3; $p = .06$ for day 5; $p = .04$ for day 7; $p = .02$ for day 9; $p = .04$ for day 11; $p = .7$ for day 13, from post hoc Tukey-Kramer test. **(F)** Similar to **(D)** for resilient mice. Main effect of reinforcement type ($F_{2,344} = 13.8$, $p = 2 \times 10^{-6}$) and day ($F_{11,344} = 3.39$, $p = 2 \times 10^{-4}$), but not for interaction ($F_{22,344} = 0.544$, $p = 1.0$), ANOVA with reinforcement type and day as fixed factors, subject as random factor. Comparisons for the c_{10} parameter vs. day −1: $p = 1.0$ for day 1; $p = 1.0$ for day 3; $p = .1$ for day 5; $p = .4$ for day 7; $p = .5$ for day 9; $p = 1.0$ for day 11; $p = 1.0$ for

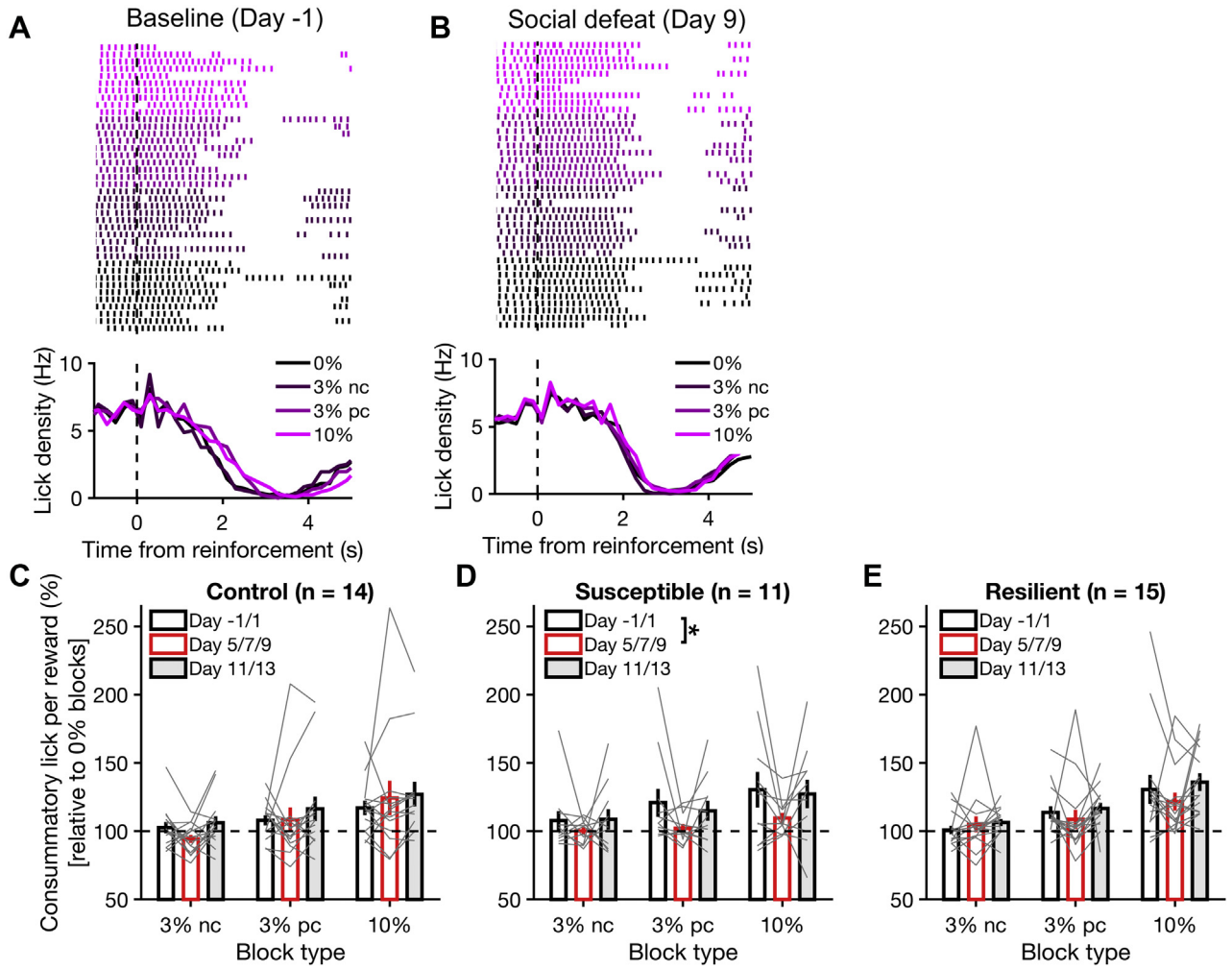

Figure 4. Chronic social defeat had only transient effect on consummatory actions. **(A**, top**)** Lick raster, chosen randomly from 10 trials of each reinforcement type from a session on day −1. (Bottom) Mean lick density relative to the time of reinforcement, plotted separately for each reinforcement type, for the same session. **(B)** Similar to **(A)** on day 9 for the same mouse. **(C)** Consummatory licks per reward for each reinforcement type, normalized by the number in 0% blocks, for control mice. For each mouse, the value was an average across days according to 3 stages: "pre" for days −1 and 1; "stress" for days 5, 7, and 9; and "post" for days 11 and 13. Gray line, individual mouse; bar, mean ± SEM. Main effect of reinforcement type ($F_{2,117}$ = 6.49, p = .002), but not for stage ($F_{2,117}$ = 0.99, p = .4) or interaction ($F_{4,117}$ = 0.28, p = .9), analysis of variance with reinforcement type and stage as fixed factors, subject as random factor. **(D)** Similar to **(C)** for susceptible mice. Main effect of reinforcement type ($F_{2,90}$ = 3.35, p = .04) and stage ($F_{2,90}$ = 3.30, p = .04), but not interaction ($F_{4,90}$ = 0.22, p = .9), with comparisons: pre vs. stress, p = .048; pre vs. post, p = .9; stress vs. post, p = .2, analysis of variance with reinforcement type and stage as fixed factors, subject as random factor, and post hoc Tukey-Kramer test. **(E)** Similar to **(C)** for resilient mice. Main effect of reinforcement type ($F_{2,126}$ = 13.3, $p = 5 \times 10^{-6}$), but not stage ($F_{2,126}$ = 1.27, p = .3) or interaction ($F_{4,126}$ = 0.39, p = .8), analysis of variance with reinforcement type and stage as fixed factors, subject as random factor. Sample sizes were 14 mice **(C, D)**, 11 mice **(E, F)**, and 15 mice **(G, H)**. *$p < .05$. nc, negative contrast; pc, positive contrast.

day 13, from post hoc Tukey-Kramer test. **(G)** The opportunity cost coefficient for the 10% sucrose reinforcement. On a mouse-by-mouse basis, the mean prestress values are plotted against the during-stress values. For susceptible mice, correlation coefficient = 0.77, p = .006. For resilient mice, correlation coefficient = 0.43, p = .1. Each circle in the scatter plot represents a mouse. Black crosshair, mean ± SEM. **(H)** The change-point parameter for the marginal utility, determined by fitting model to individual sessions for control mice. Line, mean ± SEM. Shading, days with social defeat. No effect of day ($F_{11,101}$ = 0.416, p = 1), ANOVA with day as fixed factor, subject as random factor. **(I)** Similar to **(H)** for susceptible mice. Main effect of day ($F_{10,89}$ = 3.89, $p = 3 \times 10^{-4}$), ANOVA with day as fixed factor, subject as random factor. Comparisons vs. day −1: p = 1.0 for day 1; p = .07 for day 3; p = .07 for day 5; p = .008 for day 7; p = .004 for day 9; p = .2 for day 11; p = 1.0 for day 13, from post hoc Tukey-Kramer test. **(J)** Similar to **(H)** for resilient mice. Main effect of day ($F_{11,114}$ = 5.00, $p = 3 \times 10^{-6}$), ANOVA with day as fixed factor, subject as random factor. Comparisons vs. day −1: p = 1.0 for day 1; p = .08 for day 3; p = .05 for day 5; p = .0006 for day 7; p = .0001 for day 9; p = .1 for day 11; p = 1.0 for day 13, from post hoc Tukey-Kramer test. Sample sizes were 14 mice **(D, H)**, 11 mice **(E, I)**, 15 mice **(F, J)**. *$p < .05$, **$p < .01$. nc, negative contrast; pc, positive contrast.

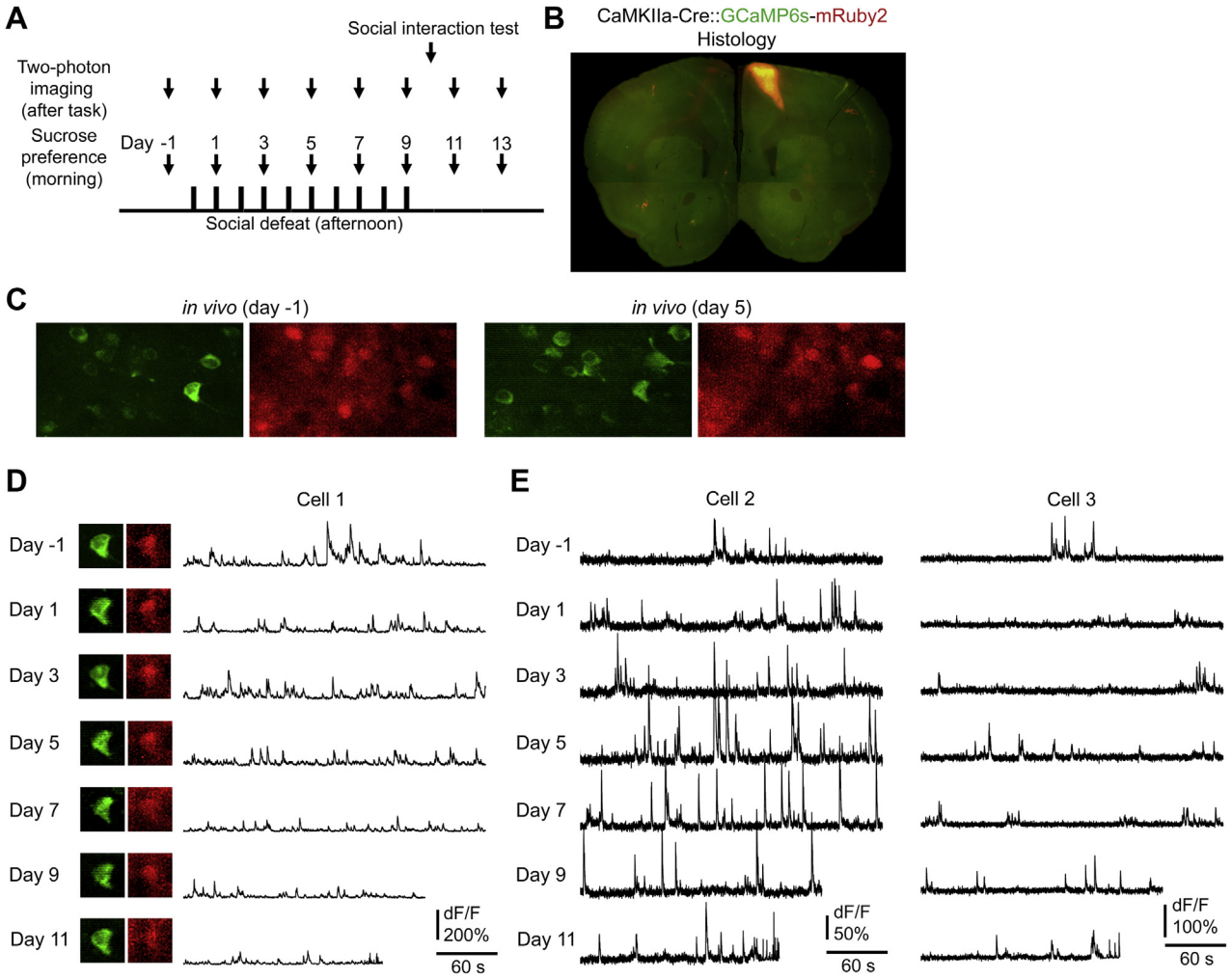

Figure 5. Longitudinal imaging of spontaneous activity of layer 2/3 pyramidal neurons in cingulate and medial secondary motor subregions. **(A)** Timeline of the experiments. **(B)** A fixed coronal section showing the extent of virally mediated expression of GCaMP6s-mRuby2 in cingulate and medial secondary motor subregions. **(C)** In vivo two-photon images from an awake, head-fixed mouse for GCaMP6s (green) and mRuby2 (red) in pyramidal neurons in cingulate and medial secondary motor subregions. The images were taken 6 days apart. **(D)** Spontaneous fluorescence transients for an example cell from **(C)**, recorded 2 days apart across 7 sessions spanning 13 days during a social defeat experiment. The insets show a still frame of the in vivo GCaMP6s and mRuby2 fluorescence on the corresponding days. **(E)** Similar to **(D)** for 2 other cells. dF/F, fractional change in fluorescence.

bicistronic vector (50) to express the genetically encoded calcium indicator GCaMP6s along with the fluorophore mRuby2 in pyramidal neurons in Cg1/M2 (Figure 5A–C; see the Supplement for experimental considerations). Using a two-photon microscope and relying on static mRuby2 fluorescence to identify cell assemblies, we could reliably track the same layer 2/3 neurons for up to 7 sessions spanning 13 days (Figure 5D, E).

Social Defeat Stress Initially Elevates the Activity of Prefrontal Pyramidal Neurons

To determine the short-term effect of social stress on Cg1/M2, we compared the spontaneously occurring calcium transients in layer 2/3 pyramidal neurons in awake mice, before versus after a single defeat (Figure 6A). Social interaction tests were used to classify the imaging mice into susceptible and resilient subtypes (Figure 6B). To infer activity rates from somatic fluorescence signals, we used a peeling algorithm based on template matching (51,52). Prior to stress, cells from the different mice had no appreciable difference in their spontaneous activity (Figure 6C). After a single defeat, susceptible mice had elevated spontaneous activity, relative to control mice (control vs. susceptible: p = .002, Wilcoxon rank-sum test) (Figure 6D). Intriguingly, resilient and control mice were indistinguishable by this measure of median activity change (control vs. resilient: p = .3, Wilcoxon rank-sum test). However, when we plotted the distribution of activity changes, a more nuanced picture arose. The distribution of the activity change was more dispersed for susceptible and resilient mice (interquartile range: 0.27 for control mice, 0.54 for susceptible, 0.47 for resilient) (Figure 6E). For resilient mice, this means that

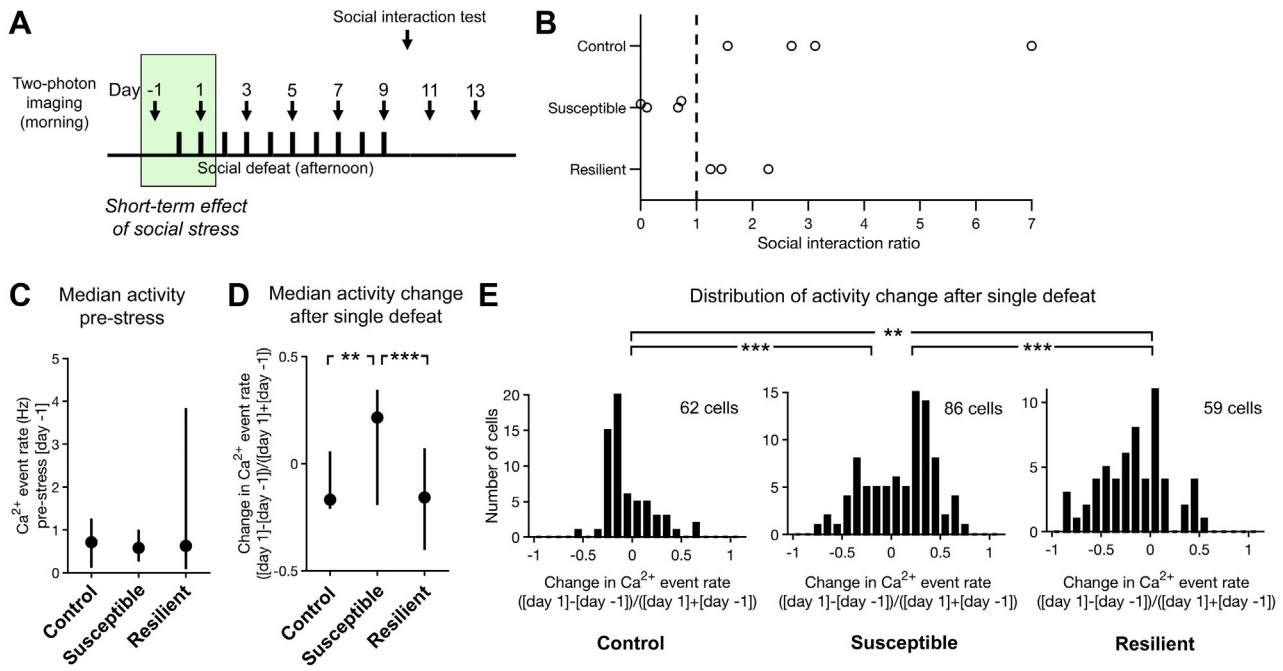

Figure 6. Social defeat rapidly alters the prefrontal cortical activity. **(A)** The timeline for experiments to determine the impact of social defeat stress on prefrontal cortical activity. The shaded green area represents the time window used for analysis of the short-term effects. **(B)** Based on the social interaction ratio, mice subjected to social defeat were divided into resilient and susceptible mice. Control mice were handled but did not experience social defeat. Each circle represents a mouse. Note that the imaging mice were a new cohort and not part of the behavior-only study. **(C)** Baseline rate of calcium events on day −1 for control, susceptible, and resilient mice. Filled circles, median; bar, 25th and 75th percentiles. Control vs. susceptible mice, $p = .6$; control vs. resilient mice, $p = .4$; susceptible vs. resilient mice, $p = .4$; Wilcoxon rank-sum test. Control vs. susceptible mice, $p = .2$; control vs. resilient mice: $p = .01$; susceptible vs. resilient mice, $p = 1 \times 10^{-4}$; Kolmogorov-Smirnov test. **(D)** Change in neural activity from day −1 to 1 for control, susceptible, and resilient mice. The activity change was a normalized difference in the rate of events inferred from fluorescence transients, calculated separately for each cell. Filled circles, median; bar, 25th and 75th percentiles. Control vs. susceptible mice, $p = .002$; control vs. resilient mice, $p = .3$; susceptible vs. resilient mice, $p = .0001$; Wilcoxon rank-sum test. **(E)** Histogram of the neural activity change from day −1 to 1 for control, susceptible, and resilient mice. Control vs. susceptible mice, $p = 2.1 \times 10^{-5}$; control vs. resilient mice, $p = .005$; susceptible vs. resilient mice, $p = 6.1 \times 10^{-6}$; Kolmogorov-Smirnov test. **(C–E)** Sample sizes were 62 cells from 4 control mice, 86 cells from 4 susceptible mice, and 59 cells from 3 resilient mice. $^{**}p < .01$, $^{***}p < .001$.

although the median did not change, there were more cells with greater decrease or increase in spontaneous activity following stress relative to control mice (control vs. resilient: $p = .005$, Kolmogorov-Smirnov test). Collectively, these results demonstrate that a single stress episode already had a detectable impact on the activity of layer 2/3 pyramidal neurons in Cg1/M2. Moreover, there is a resilience-specific compensation that dampened the overall activity after stress to be comparable to control mice.

Social Defeat Stress Exerts Heterogeneous Long-term Effects on Prefrontal Cortical Activity

We continued to image the stressed mice and, for a majority of the cells, tracked their activity throughout and beyond the social defeat manipulation (Figure 7A). Using heat maps, we could visualize and compare how the spontaneous activity levels of the same layer 2/3 pyramidal neurons in Cg1/M2 changed relative to prestress baseline (Figure 7B). We applied hierarchical clustering to agglomerate cells with similar time courses of stress-induced activity changes, which segregated into 4 major clusters: types 1, 2, 3, and 4 (Figure 7C–E; Figure S1). Type 1 cells included neurons with an initial elevation of spontaneous activity, followed by decreases for the next 2 sessions down to a sustained level below the baseline. This was the most frequently observed type of time course; cells with this profile could be found in both susceptible and resilient mice ($p = .49$, χ^2 test). Type 2 cells had a monotonic decline in spontaneous activity in response to repeated stress. The decrease continued across the initial stress sessions before stabilizing to a steady below-baseline level. Notably, type 2 cells were significantly more common in resilient mice ($p = .002$, χ^2 test). By contrast, types 3 and 4 cells were more abundant in the susceptible animals, although the comparisons did not reach statistical significance likely because there were few cells with these time courses (type 3: $p = .05$, type 4: $p = .20$, χ^2 test). Types 3 and 4 cells had a time course that was either steady near the baseline or had prolonged heighted spontaneous activity. In particular, type 4 cells might be the most related to the stress-induced motivational anhedonia, as they were predominantly found in susceptible mice (6 of 7 cells) and mirrored the progression of the behavioral deficit. The prestress activity levels of these functional cell types did not appear to predispose a mouse to be susceptible (Figure 7F). Together, these results show the stress-induced emergence of heterogeneous neural adaptations in prefrontal pyramidal neurons.

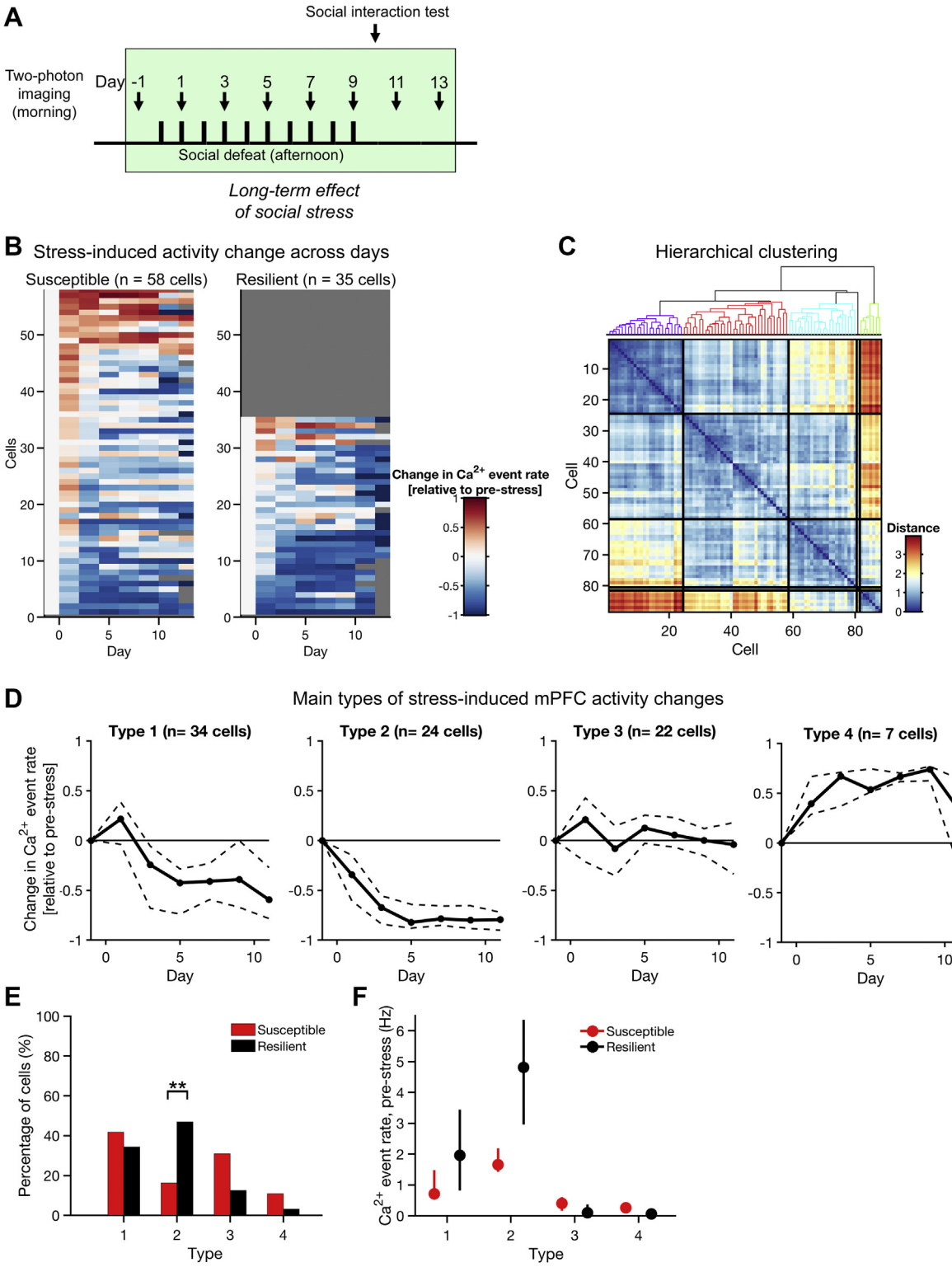

Figure 7. Social defeat induces heterogeneous long-term activity changes in the prefrontal cortex. **(A)** The timeline for experiments to determine the impact of social defeat stress on prefrontal cortical activity. The shaded green area represents the time window used for analysis of the long-term effects. **(B)** Heat maps showing the change in spontaneous activity relative to the prestress baseline. Each row is a cell. The left and right heat maps contain the 58 cells from 4 susceptible mice and 35 cells from 3 resilient mice, respectively. Red indicates an increase in spontaneous activity relative to prestress day −1. Blue indicates a decrease. **(C)** The dendrogram and pairwise similarity matrix for the hierarchical clustering with Euclidean distance as the distance metric on the entire data

DISCUSSION

In this study, we measured the longitudinal effects of repeated social defeat on reward-directed actions and determined the concomitant profiles of activity changes for layer 2/3 pyramidal neurons in Cg1/M2. There are two main findings. First, behavioral and neural deficits in response to social defeat build over multiple stress episodes. This suggests that the response to repeated stress is not a unitary behavioral condition, but rather represents a continuum where accumulating exposure progressively deteriorates reward processing. The progression was observed in behavior as well as in activity of individual neurons. Second, resilience is associated with neural activity adaptations that are not only distinct from susceptible mice, but also dissimilar from control mice. This finding raises the possibility that resilience involves the capacity to reorganize prefrontal cortical activity adaptively to counteract the negative impact of social stress.

On average across all cells, we showed an initial elevation and then subsequent reduction of spontaneous activity in prefrontal pyramidal neurons in susceptible mice. These results match well with what we know in terms of stress-induced glutamatergic dysfunction in the prefrontal cortex (53). Specifically, acute restraint stress leads to an immediate increase in extracellular glutamate recorded in the mPFC, which peaks 20 minutes after the termination of stress but continues to be elevated up to the latest data point measured at 80 minutes poststress (54). This initial hyperexcitation may underlie the increased surface levels of glutamatergic receptors, as well as potentiated synaptic responses following acute exposure to stress (55). Studies of chronic stress exposure have generally showed the opposite trend of prefrontal cortical hypoactivity. Mice subjected to 10 days of social defeat have reduced glutamate levels in the prefrontal cortex (36). A number of cellular mechanisms may underlie the reduced glutamatergic signaling, including the loss of AMPA and NMDA receptors (19), structural atrophy such as dendritic retraction and synapse loss (17,18), and maladaptive synaptic inhibition (56).

The novelty of this study is that we have measured the heterogeneous changes in cellular activity as the animal experiences successive stress episodes and develops a behavioral response to that stress. Previous studies have hinted at heterogeneous neural responses on a short-term time scale. For example, it has been reported that prefrontal cortical neurons can have either transient or protracted firing responses to restraint (57). Moreover, stress-related excitatory synaptic modifications may be selective to a subset of prefrontal cortical neurons (20). In the current study, we used hierarchical clustering to identify several major profiles of stress-induced activity changes in prefrontal cortical neurons. The most numerous neuronal subtype (type 1) displays bidirectional activity changes involving initial hyperactivity followed by sustained hypoactivity. This time course might be expected based on the glutamatergic dysfunction associated with acute and chronic stress. Interestingly, both susceptible and resilient mice had a large number of type 1 neurons, suggesting that this functional cell type may not be the distinguishing feature of susceptibility versus resilience. Instead, types 2, 3, and 4 neurons have a monotonic progression of activity changes over time, and their proportions differ depending on the mouse's reactivity to social stress. The implication is that a minor fraction of prefrontal cortical neurons may be particularly relevant for mediating the stress-induced behavioral deficits.

The progressive alterations of prefrontal cortical activity would be accompanied by the structural retraction of dendrites that have been widely documented in rodent mPFC including the Cg1/M2 areas (58,59). There is evidence to suggest that the functional and structural maladaptations may occur in lockstep. On the one hand, structural atrophy is expected to reduce dendritic excitability and diminish the firing rates of pyramidal neurons (60). On the other hand, perturbations in glutamatergic neurotransmission could induce stress-related structural remodeling in mPFC (61). The bidirectional relationship may be the basis for a positive feedback loop that promotes functional and structural neural maladaptations. Moreover, just as we showed that pyramidal neurons exhibit different types of activity changes in response to repeated social defeat, it has also been reported that stress-related dendritic remodeling can be heterogeneous across cell types. For example, among layer 2/3 pyramidal neurons in the mPFC, repeated immobilization stress caused dendritic retraction in the entorhinal cortex-projecting subpopulation, but had no effect on the amygdala-projecting subpopulation (62).

In addition to the long-term differences in time courses, we demonstrated distinct features in neural activity changes following a single defeat between susceptible and resilient mice. Intriguingly, resilient mice were different from both susceptible and control mice. At the ensemble level, resilient mice were characterized by a wide range of activity changes, yielding a median activity change that is comparable to that of control mice but significantly lower than that of susceptible mice. These observations suggest that resilience is associated with adaptations of prefrontal cortical activity that brings the overall equilibrium to a normal level. By contrast, susceptibility to social stress may represent a failure to reorganize neural activity appropriately to counteract the stress effects, leading to a hyperactive state. More experiments will be needed to relate these findings to other molecular and network mechanisms that have been suggested to confer vulnerability and resilience to social stress (63,64). The idea that resilience is not

set of 93 cells. **(D)** Cells were classified as types 1 to 4 based on the cluster membership identified by the hierarchical procedure. For each type, the change in spontaneous activity was averaged across cells. Solid line, median. Dotted lines, 20th and 80th percentiles. **(E)** Proportion of cells in susceptible or resilient mice that was classified as types 1 to 4. Comparing the proportions between susceptible and resilient mice, the difference was significant for type 2 ($p = .002$, χ^2 test) and did not reach significance for type 1 ($p = .49$), type 3 ($p = .05$), and type 4 ($p = .20$). **(F)** Baseline rate of calcium events on day −1 in susceptible or resilient mice for types 1 to 4 cells. Filled circles, median; bar, 25th and 75th percentiles. Two-way analysis of variance with factors of cell type and mouse group. Main effect of cell type ($F_{3,85} = 14.0$; $p = 2 \times 10^{-7}$), but not for mouse group ($F_{1,85} = 2.0$; $p = .2$) or interaction ($F_{3,85} = 2.0$; $p = .1$). Post hoc Tukey-Kramer comparisons: type 1 vs. 2, $p = .0005$; type 1 vs. 3, $p = .04$; type 1 vs. 4, $p = .3$; type 2 vs. 3, $p = 6 \times 10^{-7}$; type 2 vs. 4, $p = .002$; type 3 vs. 4, $p = 1$. $^{**}p < .01$. mPFC, medial prefrontal cortex.

the same as unstressed, but rather is "stressed plus neural compensations," is in agreement with the current perspective for how brain structure and connectivity in humans may adapt to early-life stress (65). Our cellular-resolution investigation provides clues for how the network-level reorganization may take shape.

To sum, the results presented here demonstrate a progressive development of behavioral and neural deficits in response to an ethologically relevant social stress. The data provide direct support for the allostatic load hypothesis, which posits that maladaptations arise from the cumulative burden of repeated stress (2). Looking ahead, a number of studies have shown that depressive-like phenotypes in rodents may be reversed by inducing synaptic plasticity in the mPFC. This may be achieved by controlling firing rates using optogenetics (13,66) or by the administration of fast-acting antidepressants such as ketamine (21,47,67). Except in a few cases (68,69), to date most studies have manipulated prefrontal pyramidal neurons indiscriminately. By showing that individual cells can have distinct profiles of activity adaptation in response to social stress, our findings suggest that neural interventions that target functional subtypes of pyramidal neurons may approximate more closely the physiological process of resilience and therefore be effective at promoting behavioral modifications.

ACKNOWLEDGMENTS AND DISCLOSURES

This work was supported by National Institutes of Health Grant Nos. R01MH112750 (to ACK), R21MH118596 (to ACK), R01MH077681 (to MRP), and DP1DA050986 (to MRP); Brain & Behavior Research Foundation Young Investigator Grant (to FB); Howard Hughes Medical Institute Medical Research Fellowship (to MH); National Institutes of Health Training Grant No. T32NS041228 (to MJS); National Science Foundation Graduate Research Fellowship DGE-1122492 (to MJS); and Alzheimer's Association Research Fellowship AARF-17-504924 (to FA).

We thank Ian Stevenson for providing code to generate the bee swarm plot.

This article was published as a preprint on bioRxiv: https://doi.org/10.1101/817361.

The authors report no biomedical financial interests or potential conflicts of interest.

ARTICLE INFORMATION

From the Department of Psychiatry (FB, MYH, FA, YSM, MRP, ACK), Interdepartmental Neuroscience Program (MJS, MRP, ACK), and Department of Neuroscience (MRP, ACK), Yale University School of Medicine, New Haven, Connecticut.

Address correspondence to Alex C. Kwan, Ph.D., Yale University, Psychiatry, 300 George Street, Suite 901, New Haven, CT 06511; E-mail: alex.kwan@yale.edu.

Received Nov 5, 2019; revised Jan 27, 2020; accepted Feb 9, 2020.

Supplementary material cited in this article is available online at https://doi.org/10.1016/j.biopsych.2020.02.008.

REFERENCES

1. Kendler KS, Karkowski LM, Prescott CA (1999): Causal relationship between stressful life events and the onset of major depression. Am J Psychiatry 156:837–841.
2. McEwen BS (2004): Protection and damage from acute and chronic stress: Allostasis and allostatic overload and relevance to the pathophysiology of psychiatric disorders. Ann N Y Acad Sci 1032:1–7.
3. McEwen BS, Stellar E (1993): Stress and the individual: Mechanisms leading to disease. Arch Intern Med 153:2093–2101.
4. Arnsten AF (2009): Stress signalling pathways that impair prefrontal cortex structure and function. Nat Rev Neurosci 10:410–422.
5. Hollon NG, Burgeno LM, Phillips PE (2015): Stress effects on the neural substrates of motivated behavior. Nat Neurosci 18:1405–1412.
6. Griffiths KR, Morris RW, Balleine BW (2014): Translational studies of goal-directed action as a framework for classifying deficits across psychiatric disorders. Front Syst Neurosci 8:101.
7. Schwabe L, Wolf OT (2009): Stress prompts habit behavior in humans. J Neurosci 29:7191–7198.
8. Dias-Ferreira E, Sousa JC, Melo I, Morgado P, Mesquita AR, Cerqueira JJ, *et al.* (2009): Chronic stress causes frontostriatal reorganization and affects decision-making. Science 325:621–625.
9. Cerqueira JJ, Mailliet F, Almeida OF, Jay TM, Sousa N (2007): The prefrontal cortex as a key target of the maladaptive response to stress. J Neurosci 27:2781–2787.
10. Der-Avakian A, Mazei-Robison MS, Kesby JP, Nestler EJ, Markou A (2014): Enduring deficits in brain reward function after chronic social defeat in rats: Susceptibility, resilience, and antidepressant response. Biol Psychiatry 76:542–549.
11. Donahue RJ, Muschamp JW, Russo SJ, Nestler EJ, Carlezon WA Jr (2014): Effects of striatal DeltaFosB overexpression and ketamine on social defeat stress-induced anhedonia in mice. Biol Psychiatry 76:550–558.
12. Krishnan V, Han MH, Graham DL, Berton O, Renthal W, Russo SJ, *et al.* (2007): Molecular adaptations underlying susceptibility and resistance to social defeat in brain reward regions. Cell 131:391–404.
13. Covington HE 3rd, Lobo MK, Maze I, Vialou V, Hyman JM, Zaman S, *et al.* (2010): Antidepressant effect of optogenetic stimulation of the medial prefrontal cortex. J Neurosci 30:16082–16090.
14. Treadway MT, Zald DH (2011): Reconsidering anhedonia in depression: Lessons from translational neuroscience. Neurosci Biobehav Rev 35:537–555.
15. Salamone JD, Correa M (2012): The mysterious motivational functions of mesolimbic dopamine. Neuron 76:470–485.
16. Chaouloff F (2013): Social stress models in depression research: What do they tell us? Cell Tissue Res 354:179–190.
17. Radley JJ, Rocher AB, Miller M, Janssen WG, Liston C, Hof PR, *et al.* (2006): Repeated stress induces dendritic spine loss in the rat medial prefrontal cortex. Cereb Cortex 16:313–320.
18. Cook SC, Wellman CL (2004): Chronic stress alters dendritic morphology in rat medial prefrontal cortex. J Neurobiol 60:236–248.
19. Yuen EY, Wei J, Liu W, Zhong P, Li X, Yan Z (2012): Repeated stress causes cognitive impairment by suppressing glutamate receptor expression and function in prefrontal cortex. Neuron 73:962–977.
20. Wang M, Perova Z, Arenkiel BR, Li B (2014): Synaptic modifications in the medial prefrontal cortex in susceptibility and resilience to stress. J Neurosci 34:7485–7492.
21. Moda-Sava RN, Murdock MH, Parekh PK, Fetcho RN, Huang BS, Huynh TN, *et al.* (2019): Sustained rescue of prefrontal circuit dysfunction by antidepressant-induced spine formation. Science 364.
22. Wilber AA, Walker AG, Southwood CJ, Farrell MR, Lin GL, Rebec GV, *et al.* (2011): Chronic stress alters neural activity in medial prefrontal cortex during retrieval of extinction. Neuroscience 174:115–131.
23. Kumar S, Hultman R, Hughes D, Michel N, Katz BM, Dzirasa K (2014): Prefrontal cortex reactivity underlies trait vulnerability to chronic social defeat stress. Nat Commun 5:4537.
24. Abe R, Okada S, Nakayama R, Ikegaya Y, Sasaki T (2019): Social defeat stress causes selective attenuation of neuronal activity in the ventromedial prefrontal cortex. Sci Rep 9:9447.
25. Ali F, Shao LX, Gerhard DM, Sweasy K, Pothula S, Pittenger C, *et al.* (2020): Inhibitory regulation of calcium transients in prefrontal dendritic spines is compromised by a nonsense Shank3 mutation [published online ahead of print March 11]. Mol Psychiatry.
26. Siniscalchi MJ, Wang H, Kwan AC (2019): Enhanced population coding for rewarded choices in the medial frontal cortex of the mouse. Cereb Cortex 29:4090–4106.
27. Mineur YS, Fote GM, Blakeman S, Cahuzac EL, Newbold SA, Picciotto MR (2016): Multiple nicotinic acetylcholine receptor subtypes in the mouse amygdala regulate affective behaviors and response to social stress. Neuropsychopharmacology 41:1579–1587.

28. Golden SA, Covington HE 3rd, Berton O, Russo SJ (2011): A standardized protocol for repeated social defeat stress in mice. Nat Protoc 6:1183–1191.
29. Dickinson A, Nicholas DJ, Adams CD (1983): The effect of the instrumental training contingency on susceptibility to reinforcer devaluation. Q J Exp Psychol B 35:35–51.
30. Flaherty CF (1982): Incentive contrast—A review of behavioral changes following shifts in reward. Anim Learn Behav 10:409–440.
31. Parent MA, Amarante LM, Liu B, Weikum D, Laubach M (2015): The medial prefrontal cortex is crucial for the maintenance of persistent licking and the expression of incentive contrast. Front Integr Neurosci 9:23.
32. Dombeck DA, Khabbaz AN, Collman F, Adelman TL, Tank DW (2007): Imaging large-scale neural activity with cellular resolution in awake, mobile mice. Neuron 56:43–57.
33. Flaherty CF, Checke S (1982): Anticipation of incentive gain. Anim Learn Behav 10:177–182.
34. Dwyer DM (2012): Licking and liking: The assessment of hedonic responses in rodents. Q J Exp Psychol (Hove) 65:371–394.
35. Davis JD, Smith GP (1992): Analysis of the microstructure of the rhythmic tongue movements of rats ingesting maltose and sucrose solutions. Behav Neurosci 106:217–228.
36. Veeraiah P, Noronha JM, Maitra S, Bagga P, Khandelwal N, Chakravarty S, *et al.* (2014): Dysfunctional glutamatergic and gamma-aminobutyric acidergic activities in prefrontal cortex of mice in social defeat model of depression. Biol Psychiatry 76:231–238.
37. Niv Y, Daw ND, Joel D, Dayan P (2007): Tonic dopamine: Opportunity costs and the control of response vigor. Psychopharmacology (Berl) 191:507–520.
38. Cools R, Nakamura K, Daw ND (2011): Serotonin and dopamine: Unifying affective, activational, and decision functions. Neuropsychopharmacology 36:98–113.
39. Barthas F, Kwan AC (2017): Secondary motor cortex: Where "sensory" meets "motor" in the rodent frontal cortex. Trends Neurosci 40:181–193.
40. Murakami M, Vicente MI, Costa GM, Mainen ZF (2014): Neural antecedents of self-initiated actions in secondary motor cortex. Nat Neurosci 17:1574–1582.
41. Murakami M, Shteingart H, Loewenstein Y, Mainen ZF (2017): Distinct sources of deterministic and stochastic components of action timing decisions in rodent frontal cortex. Neuron 94:908–919.e907.
42. Siniscalchi MJ, Phoumthipphavong V, Ali F, Lozano M, Kwan AC (2016): Fast and slow transitions in frontal ensemble activity during flexible sensorimotor behavior. Nat Neurosci 19:1234–1242.
43. Sul JH, Jo S, Lee D, Jung MW (2011): Role of rodent secondary motor cortex in value-based action selection. Nat Neurosci 14:1202–1208.
44. Gremel CM, Costa RM (2013): Premotor cortex is critical for goal-directed actions. Front Comput Neurosci 7:110.
45. Kim Y, Perova Z, Mirrione MM, Pradhan K, Henn FA, Shea S, *et al.* (2016): Whole-brain mapping of neuronal activity in the learned helplessness model of depression. Front Neural Circuits 10:3.
46. Miyamoto S, Mailman RB, Lieberman JA, Duncan GE (2001): Blunted brain metabolic response to ketamine in mice lacking D(1A) dopamine receptors. Brain Res 894:167–180.
47. Phoumthipphavong V, Barthas F, Hassett S, Kwan AC (2016): Longitudinal effects of ketamine on dendritic architecture in vivo in the mouse medial frontal cortex. eNeuro 3. ENEURO.0133-15.2016.
48. Ali F, Gerhard DM, Sweasy K, Pothula S, Pittenger C, Duman RS, *et al.* (2020): Ketamine disinhibits dendrites and enhances calcium signals in prefrontal dendritic spines. Nat Commun 11:72.
49. Ali F, Kwan AC (2020): Interpreting in vivo calcium signals from neuronal cell bodies, axons, and dendrites: A review. Neurophotonics 7:011402.
50. Rose T, Jaepel J, Hubener M, Bonhoeffer T (2016): Cell-specific restoration of stimulus preference after monocular deprivation in the visual cortex. Science 352:1319–1322.
51. Grewe BF, Langer D, Kasper H, Kampa BM, Helmchen F (2010): High-speed in vivo calcium imaging reveals neuronal network activity with near-millisecond precision. Nat Methods 7:399–405.
52. Lutcke H, Gerhard F, Zenke F, Gerstner W, Helmchen F (2013): Inference of neuronal network spike dynamics and topology from calcium imaging data. Front Neural Circuits 7:201.
53. Popoli M, Yan Z, McEwen BS, Sanacora G (2011): The stressed synapse: The impact of stress and glucocorticoids on glutamate transmission. Nat Rev Neurosci 13:22–37.
54. Moghaddam B (1993): Stress preferentially increases extraneuronal levels of excitatory amino acids in the prefrontal cortex: Comparison to hippocampus and basal ganglia. J Neurochem 60:1650–1657.
55. Yuen EY, Liu W, Karatsoreos IN, Ren Y, Feng J, McEwen BS, *et al.* (2011): Mechanisms for acute stress-induced enhancement of glutamatergic transmission and working memory. Mol Psychiatry 16:156–170.
56. McKlveen JM, Morano RL, Fitzgerald M, Zoubovsky S, Cassella SN, Scheimann JR, *et al.* (2016): Chronic stress increases prefrontal inhibition: A mechanism for stress-induced prefrontal dysfunction. Biol Psychiatry 80:754–764.
57. Jackson ME, Moghaddam B (2006): Distinct patterns of plasticity in prefrontal cortex neurons that encode slow and fast responses to stress. Eur J Neurosci 24:1702–1710.
58. Radley JJ, Sisti HM, Hao J, Rocher AB, McCall T, Hof PR, *et al.* (2004): Chronic behavioral stress induces apical dendritic reorganization in pyramidal neurons of the medial prefrontal cortex. Neuroscience 125:1–6.
59. Liston C, Miller MM, Goldwater DS, Radley JJ, Rocher AB, Hof PR, *et al.* (2006): Stress-induced alterations in prefrontal cortical dendritic morphology predict selective impairments in perceptual attentional set-shifting. J Neurosci 26:7870–7874.
60. Liu RJ, Aghajanian GK (2008): Stress blunts serotonin- and hypocretin-evoked EPSCs in prefrontal cortex: Role of corticosterone-mediated apical dendritic atrophy. Proc Natl Acad Sci U S A 105:359–364.
61. Martin KP, Wellman CL (2011): NMDA receptor blockade alters stress-induced dendritic remodeling in medial prefrontal cortex. Cereb Cortex 21:2366–2373.
62. Shansky RM, Hamo C, Hof PR, McEwen BS, Morrison JH (2009): Stress-induced dendritic remodeling in the prefrontal cortex is circuit specific. Cereb Cortex 19:2479–2484.
63. Bagot RC, Cates HM, Purushothaman I, Lorsch ZS, Walker DM, Wang J, *et al.* (2016): Circuit-wide transcriptional profiling reveals brain region-specific gene networks regulating depression susceptibility. Neuron 90:969–983.
64. Hultman R, Ulrich K, Sachs BD, Blount C, Carlson DE, Ndubuizu N, *et al.* (2018): Brain-wide electrical spatiotemporal dynamics encode depression vulnerability. Cell 173:166–180.e114.
65. Teicher MH, Samson JA, Anderson CM, Ohashi K (2016): The effects of childhood maltreatment on brain structure, function and connectivity. Nat Rev Neurosci 17:652–666.
66. Fuchikami M, Thomas A, Liu R, Wohleb ES, Land BB, DiLeone RJ, *et al.* (2015): Optogenetic stimulation of infralimbic PFC reproduces ketamine's rapid and sustained antidepressant actions. Proc Natl Acad Sci U S A 112:8106–8111.
67. Li N, Lee B, Liu RJ, Banasr M, Dwyer JM, Iwata M, *et al.* (2010): mTOR-dependent synapse formation underlies the rapid antidepressant effects of NMDA antagonists. Science 329:959–964.
68. Warden MR, Selimbeyoglu A, Mirzabekov JJ, Lo M, Thompson KR, Kim SY, *et al.* (2012): A prefrontal cortex-brainstem neuronal projection that controls response to behavioural challenge. Nature 492:428–432.
69. Hare BD, Shinohara R, Liu RJ, Pothula S, DiLeone RJ, Duman RS (2019): Optogenetic stimulation of medial prefrontal cortex Drd1 neurons produces rapid and long-lasting antidepressant effects. Nat Commun 10:223.